ISSN (Print) 1226-1750
ISSN (Online) 2233-6656
Journal of Magnetics 23(1), 106-111 (2018) https://doi.org/10.4283/JMAG.2018.23.1.106

Structural and Magnetic Properties of Aluminium-Substituted Cobalt-Ferrite Nanoparticles Synthesised by the Co-precipitation Route

Budi Purnama*, Anisa Khoiriah, and Suharyana

Department of Physics, Faculty of Math and Natural Sciences Sebelas Maret University, Jl. Ir. Sutami 36A Kentingan Surakarta 57126, Indonesia

(Received 14 October 2017, Received in final form 21 January 2018, Accepted 23 January 2018)

The crystal structure and magnetic properties of aluminium-substituted cobalt-ferrite nanoparticles synthesised by the co-precipitation are reported in this study. The single phase nanoparticles are obtained. Magnetic property Changes in these properties are clarified mainly by changes in parameters such as the crystalline constant, crystallite size and crystalline density. An increase of saturated magnetisation with annealing temperature is also observed. Results for the change in saturated magnetization at several elevated temperatures indicate that the available non-magnetic aluminium ions support redistribution of cation-trivalent Fe^{3+} during the annealing process at octahedral sites.

Keywords : cobalt ferrite, aluminium, co-precipitation, nanoparticles

1. Introduction

Cobalt-ferrite-based nanoparticles are fascinating magnetic materials that have been widely studied over the last decade. This material does not lose its magnetic properties despite its nanometre-order particle size. Moreover, the magnetic characteristics of these nanoparticles can be modified by substitution of non-magnetic metal ions and rare-earth metals, because the crystalline structure of the inverse spinel in cobalt-ferrite-based materials allows the possibility of cation redistribution in octahedral and tetragonal sites. In these nanoparticles, divalent cations occupy octahedral sites and trivalent cations can occupy both octahedral and tetrahedral sites [1]. Aluminium is one such trivalent-cationic metal that used as doping in cobalt ferrite nano particles system [2-13]. In general, the increase of aluminium cations in the cobalt-ferrite-nanoparticle structure will modify the magnetic characteristics by changing the crystallite size [6], crystalline density [3, 4], effective bond lengths [3] and lattice constant [2-4, 6]. Kuanr *et al.* have explained the decrease in saturated magnetisation in terms of the magnetic-dilution effect [6]. There is also evidence that the availability of aluminium cations causes domain wall [7]. In terms of the fundamental electrical properties, increasing Al content enhances the energy gap [9]. The aluminium content of the cobalt-ferrite nanoparticles also decreases the Curie Temperature [2, 10]. A recent study experimentally confirmed that aluminium cations can be substituted for Fe^{3+} cations at both octahedral and tetrahedral sites [12]. Due to its interesting properties, alumunium-substituted cobalt ferrite allows high-frequency-device applications [11] and its use as a nano-absorbent in aqueous systems cannot be ruled out [13].

In previous research, almost all aluminium-substituted cobalt ferrite has been synthesised at low temperatures following post-heating treatment at a moderate temperature. In this study, the structural and magnetic characteristics of co-precipitated aluminium-substituted cobalt-ferrite nanoparticles are presented. Post-annealing samples are selected for elevated temperatures to promote redistribution of cations. The resulting cobalt-ferrite nanoparticles are characterised using TG/DTA, FTIR, X-ray diffraction (XRD), SEM and a vibrating-sample magnetometer (VSM).

2. Experiment

Aluminium-substituted cobalt-ferrite nanoparticles, $CoAl_xFe_{2-x}O_4$, with $x = 0$, 0.01 and 0.1, are synthesised by the co-precipitation method. $Co(NO_3)_2{\cdot}6H_2O$ (Merck), $Fe(NO_3)_3{\cdot}9H_2O$ (Merck), $Al(NO_3)_3{\cdot}9H_2O$ (Merck) and

*Corresponding author: Tel: +62-271-669017
Fax: +62-271-669017, e-mail: bpurnama@mipa.uns.ac.id

NaOH (Merck) are used without further purification. The synthesis procedure followed as reported else where [14]. Next, the product samples were annealed at temperatures of 600 °C, 800 °C and 1,000 °C under atmospheric conditions for 5 h. The FTIR was used to study the spinel structure of the material.. The crystalline structures of the final samples were characterised by the XRD by using a Bruker D8 Advance system using CuKα-source (1.54 Å) radiation. The crystallite size (D)- of the aluminium-substituted cobalt-ferrite nanoparticles was calculated by employing Scherrer's equation at its strongest peak, $D = 0.9\ \lambda/(\beta\cos\theta)$, where λ is the wavelength of the X-ray radiation, θ is the Braggs' angle and β is the full width at half maximum (FWHM). The lattice constant, a, was evaluated using the equation $a = \frac{\lambda}{2\sin\theta}\sqrt{h^2+k^2+l^2}$ (with h, k and l being the Miller indices). The crystalline density ρ was calculated using $\rho = Z{\cdot}M/N_A{\cdot}a^3$, where Z is the number of molecules per cell, M is the molecular weight and N_A is Avogadro's number [15]. The magnetic properties were evaluated using a VSM at room temperature with a scan range from −20 kOe to 20 kOe.

3. Experimental Results

Figure 1 shows FTIR spectra for the aluminium-substituted cobalt-ferrite nanoparticles of $CoAl_xFe_{2-x}O_4$ with x = 0, 0.01 and 0.1. The nanoparticle samples were synthesized using the co-precipitation method followed by post-annealing treatment at a temperature of 600 °C for 5 h under atmospheric conditions. In a co-precipitated sample, without aluminium substitution (*i.e.* $x = 0$), the O–H bond was indicated by a broader absorption peak at a wavenumber of 3,420 cm^{-1}, whereas, for aluminium-substituted cobalt ferrite with $x = 0.01$ and 0.1, the sharp absorbance curves of the O–H bond appeared at wave-numbers of 3,441 cm^{-1} and 3,420 cm^{-1} respectively. The decrease of the absorption peak near 3400 cm^{-1} indicate that the O–H bond become lost at high temperature. Furthermore, the absorption peak was around 1,600 cm^{-1}, suggesting the stretching of the C=O bond. At around a wavenumber of $k = 990$ cm^{-1}, a characteristic absorbance peak appeared. This peak was not seen in the original cobalt=ferrite nanoparticles and resulted from stretching of the metal oxide, which was suggested as aluminium ions were substituted into cobalt ferrite. Finally, the metal-oxide bonds of cobalt ferrite appeared as an absorption peak around 590 cm^{-1} in the FTIR spectrum. Interestingly, there was no significant change of the wavenumber in the original cobalt-ferrite nanoparticle with the increase of aluminium-ion content. This suggests that aluminium was substituted into cobalt-ferrite nanoparticles.

The FTIR curves of the aluminium-substituted cobalt-ferrite nanoparticles subjected to 5 hours of annealing at temperatures of 600 °C, 800 °C and 1,000 °C under atmospheric conditions are depicted in Fig. 2. Here, the molar concentration of aluminium is selected to be $x = 0.1$ in $CoAl_xFe_{2-x}O_4$. The three typical absorption peaks mentioned in the previous discussion are recognised in the curve. The first peaks occur at wavenumbers of 3,421 cm^{-1}, 3,485 cm^{-1} and 3,418 cm^{-1} for the 600 °C, 800 °C and 1,000 °C cases, respectively. The stretching mode and

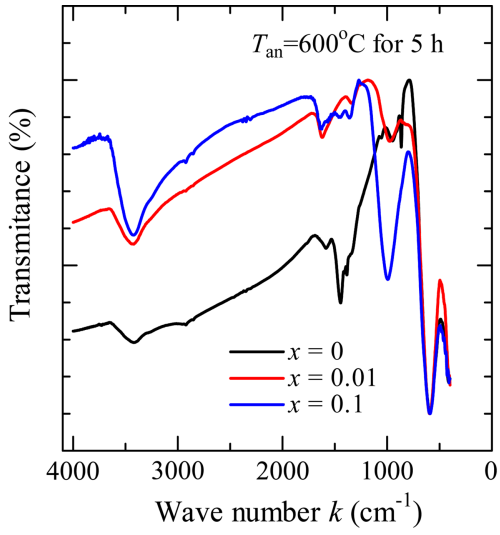

Fig. 1. (Color online) Typical FTIR results for aluminium-substituted cobalt-ferrite nanoparticles, $CoAl_xFe_{2-x}O_4$, with x = 0, 0.01 and 0.1.

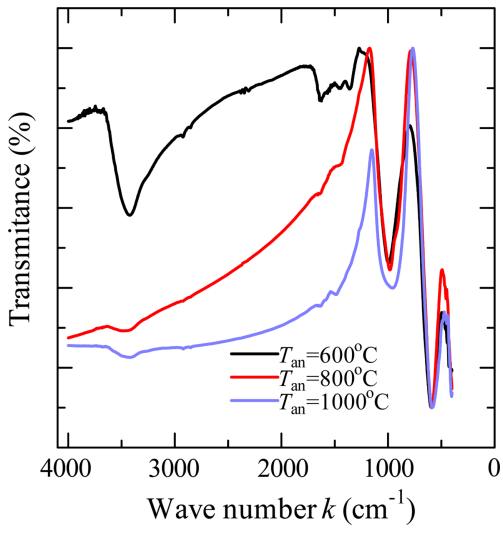

Fig. 2. (Color online) Typical FTIR spectra of aluminium-substituted cobalt-ferrite nanoparticles, $CoAl_xFe_{2-x}O_4$, with x = 0.1.

the H–O–H bending vibration contribute to the absorption peak. The second absorption peaks occur at wavenumbers of 995.31 cm^{-1}, 981.81 cm^{-1} and 950.95 cm^{-1} for 600 °C, 800 °C and 1,000 °C, respectively. These results are thought to be due to the presence of aluminium ions in the cobalt-ferrite-nanoparticle system. It is clear that the absorption peak increases with the increase of the annealing temperature. This indicates that the substitution of aluminium ions into cobalt-ferrite nanoparticles is thermally stable, meaning that the heat energy received by an increasing annealing temperature is only used to redistribute the aluminium ions in the cobalt-ferrite-nanoparticle structure. This has been confirmed from the XRD pattern analysis. The third absorption peaks occur at wavenumbers of 590.24 cm^{-1}, 591.21 cm^{-1} and 584.46 cm^{-1} for 600 °C, 800 °C and 1,000 °C respectively. The peak observed near 590 cm^{-1} is a common feature in spinel ferrite oxide and is attributed to the intrinsic vibration of A-site metal complexes, which consist of bonds between A-site metal ions and oxygen ions. This confirms the appearance of $CoFe_2O_4$ synthesised by the co-precipitation route. The absorption band near 590 cm^{-1} is consistent with an increase in the annealing temperature. In order to obtain a more detailed explanation of the annealing temperature's effect upon the aluminium-substituted cobalt-ferrite nanoparticles, we characterised the samples using powder X-ray diffractometry.

The XRD patterns of $CoAl_xFe_{2-x}O_4$ with $x = 0$, 0.01 and 0.1 are depicted in Fig. 3. The samples were annealed at a temperature of 600 °C under atmospheric conditions for 5 h. It can be clearly observed that the strongest peak is

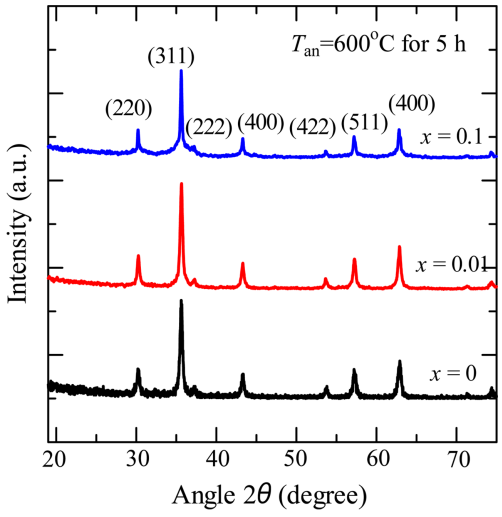

Fig. 3. (Color online) XRD patterns for aluminium-substituted cobalt-ferrite $CoAl_xFe_{2-x}O_4$ nanoparticles for aluminium compositions of $x = 0$, 0.01 and 0.1 at an annealing temperature of 600 °C for 5 h.

Table 1. Calculated crystallite size D, lattice distance a and crystalline density ρ of aluminium substituted cobalt ferrite nanoparticles annealed at 600 °C for 5 hours.

	Variation aluminium content $CoAl_xFe_{2-x}O_4$		
	$x = 0$	$x = 0.01$	$x = 0$, 1
Crystallite size D (nm)	24.55	26.09	29.79
Parameter a (Å)	8.36	8.36	8.35
Density ρ (g/cm^3)	5.34	5.35	5.36

independent of the aluminium-ion concentration and consistently appears at an angle of $2\theta = 35.61°$. Thus, the strongest peak is not significantly reduced with the increase of the aluminium content. The other characteristic peaks of spinel ferrite in the XRD pattern, which indicate the presence of aluminium oxides or other impurities in the sample, are absent within the XRD technique limit. Therefore, aluminium-substituted cobalt-ferrite nanoparticles were successfully produced by the co-precipitation method. The crystallite sizes (D), lattice spacing (a) and crystalline density (ρ) obtained using the highest intensity XRD peak are listed in Table 1.

It can also be observed that the crystallite size increases with the increase of the aluminium content in the nanoparticles. Using the strongest XRD peak and the Scherrer formula, crystallite sizes of 24, 26 and 35 nm were obtained for the aluminium-substituted cobalt-ferrite nanoparticles corresponding to aluminium contents of $x = 0$, 0.01 and 0.10, respectively. The crystallite density ρ for the aluminium-substituted cobalt ferrite slightly increased with increasing aluminium. Crystallite densities of 5.34, 5.35 and 5.36 g/cm^3 were calculated for the aluminium-substituted cobalt-ferrite nanoparticles with $x = 0$, 0.01 and 0.1, respectively. This is due to the inter-ionic distance becoming shorter with the increase of aluminium [4]. This result was also reflected in the lattice-constant parameter a, which slightly decreased from 8.36 to 8.35 Å as the aluminium content increased from $x = 0$ to $x = 0.1$.

The XRD patterns of $CoAl_xFe_{2-x}O_4$, with $x = 0.1$ and annealed at different temperatures are depicted in Fig. 4. The crystallite sizes D, lattice constant a and crystalline

Table 2. Crystallite size (D), lattice constant a and crystalline density ρ for aluminium substituted cobalt ferrite nanoparticles annealed at 600 °C for 5 hours.

	$CoAl_xFe_{2-x}O_4$ with $x = 0.1$		
Temperature annealing	600 °C	800 °C	1,000 °C
Crystallite size D (nm)	34.78	32.09	29.79
Parameter a (Å)	8.35	8.39	8.39
Density ρ (g/cm^3)	5.34	5.27	5.27

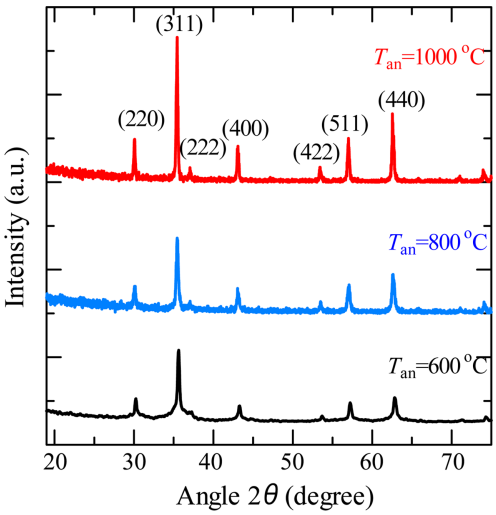

Fig. 4. (Color online) XRD patterns for aluminium-substituted cobalt-ferrite nanoparticles at annealing.

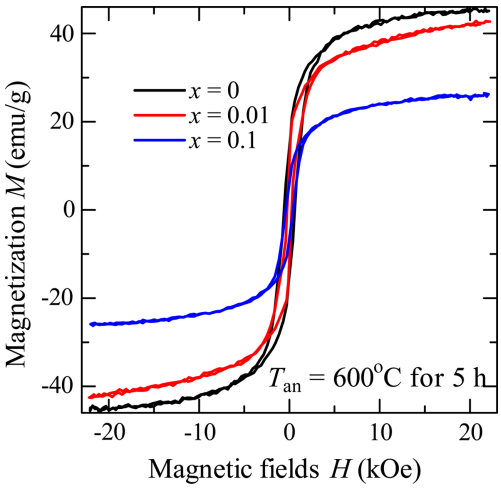

Fig. 5. (Color online) M-H hysteresis curves of $CoAl_xFe_{2-x}O_4$ for x = 0, 0.01 and 0.1 annealed at 600 °C for 5 h.

density ρ obtained by using the highest intensity XRD peak and the Scherrer's formula are listed in Table 2. The samples were annealed at temperatures of 600 °C, 800 °C and 1,000 °C under atmospheric conditions for 5 h. It can be clearly observed that the strongest peak increased along with the annealing temperature. The thermal energy from the annealing temperature is used to refine the crystallite structure. The parameter a and density ρ values of 8.39 Å and 5.27 g/cm^3 respectively are well matched with the ICDD number 221086. crystallite size of 34.78 nm was obtained for annealing at 600 °C and it becomes 32.09 nm and 29.79 nm for annealing temperatures of 800 °C and 1,000 °C respectively. The decrease of D was a consequence of the decrease in density [9]. Furthermore, the thermal energy is used to redistribute cations at crystallite sites, which will be shown later to be reflected in changes to the magnetic properties.

Figure 5 shows the magnetisation curve (M-H hysteresis loop) for $CoAl_xFe_{2-x}O_4$ with $x = 0$, 0.01 and 0.1. The samples are annealed at a temperature of 600 °C for 5 h under atmospheric conditions. It can be clearly observed in the figure that the increase of the aluminium content decreases the saturation magnetisation, which is 45.61 emu/g for the sample without aluminium. For $x = 0.01$ and $x = 0.1$, the saturation magnetisation decreases to 42.84 emu/g and 26.46 emu/g, respectively. The preference of the net magnetic moment of a cobalt-ferrite nanoparticle with the present spinel structure is given as [16] $m = \Sigma m_{\text{octahedral}} - \Sigma m_{\text{tetrahedral}}$ due to the opposite preference orientation of the magnetic moments for both octahedral and tetrahedral sites [1]. It should be noted that trivalent cations are distributed at octahedral and tetrahedral sites, whereas divalent cations have a preference for octahedral sites. Furthermore, the preference the magnetic moment A reduction of the saturation magnetisation should occur as aluminium ions replace the original trivalent Fe cations at octahedral sites. These results are consistent with those previously reported by Anantharamaiah and Joy [12]. The coercive field assumes different expressions for various aluminium contents. The coercive field, H_C, does not indicate a preference for any trend. It is 590.38 Oe for x = 0, becoming 250.00 Oe and 414.04 Oe for $x = 0.01$ and 0.1 respectively.

The M-H hysteresis loops for $CoAl_xFe_{2-x}O_4$ with x = 0.1, annealed at 600 °C, 800 °C and 1,000 °C are depicted in Fig. 6. It is clear that the saturate magnetisation consistently increases along with the annealing temperature.

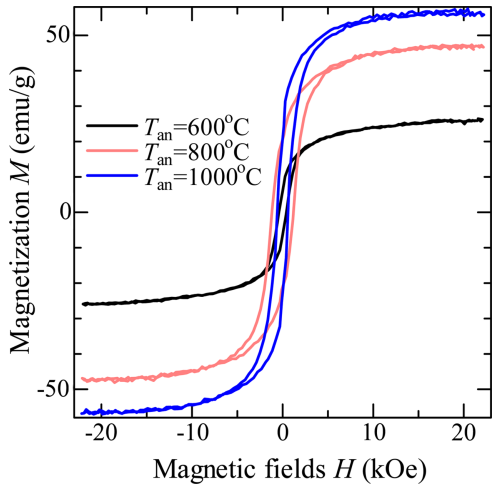

Fig. 6. (Color online) Hysteresis curves for aluminium cobalt-ferrite nanoparticles at annealing temperatures of 600 °C, 800 °C and 1,000 °C for 5 h.

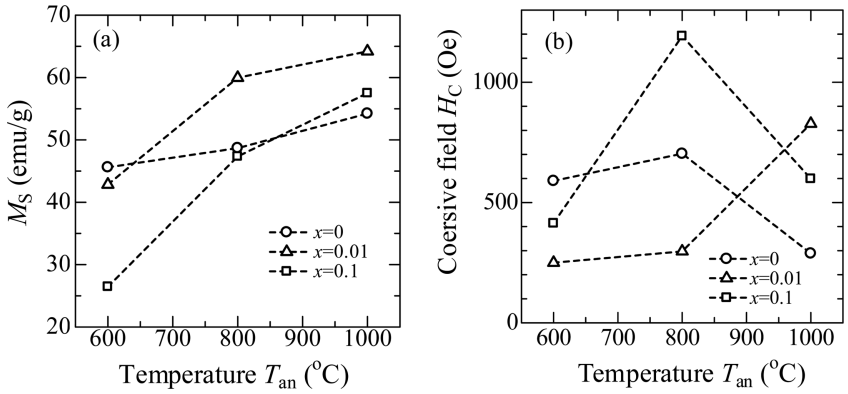

Fig. 7. (a) The saturated magnetisation, M_S, and (b) the coercive field, H_C, as functions of temperature for 5 h of annealing under atmospheric conditions in aluminium-substituted cobalt ferrite ($CoAl_xFe_{2-x}O_4$) with x = 0, 0.01 and 0.1.

The coercive field, H_C, also changes with the increase in temperature. The saturated magnetisations were 26.46 emu/g, 47.34 emu/g and 57.50 emu/g for the 600 °C, 800 °C and 1,000 °C respectively. As discussed previously, the preference of the net magnetic moment is defined as the difference in the cation distributions at the octahedral and tetrahedral sites. The increase of the saturated magnetisation with annealing temperature should be attributed to the redistribution of trivalent Fe cations at octahedral sites. Moreover, a coercive field of 414.04 Oe is attained for an annealing temperature of 600 °C. Then, H_C drastically increases to 1,192.02 Oe for an annealing temperature of 800 °C. Thereafter, H_C decreases to 598.70 Oe for an annealing temperature of 1,000 °C. The saturation magnetisation and coercive field results in aluminium-substituted cobalt ferrite for various annealing temperatures are presented in Fig. 7.

Figure 7 shows the temperature dependence of (a) the saturated magnetisation, M_S, and (b) the coercive field, H_C, in aluminium-substituted cobalt ferrite after post-annealing for 5 h. Figure 7(a) confirms that the saturated magnetisation increases along with annealing temperature for the whole aluminium content. When the presence of aluminum ions provides a greater chance of cation re-distribution is discussed then the redistribution of divalent cation occupying the octahedral sites will increase the saturation magnetization. In the case of cobalt-ferrite nanoparticles without aluminium, the increase in saturated magnetisation between annealing temperatures of 600 °C and 1,000 °C is equal to 86.1 emu/g (= 542.2-456.1). Contrarily, for $CoAl_xFe_{2-x}O_4$ with x = 0.01, the change in saturated magnetisation is equal to 213.9 emu/g (= 642.1-428.4) and becomes 548.54 emu/g (= 575-26.46) for x = 0.1. The smallest change of the saturation magnetisation occurs for cobalt-ferrite nanoparticles without aluminium content and the largest change of the saturated magnetisation occurs for x = 0.1. The obtained data confirm that the available non-magnetic aluminium ions support the redistribution of cations during the annealing process at octahedral sites.

In contrast to saturated magnetisation, the annealing-temperature dependence of the coercive field is not simple. Samples with and without aluminium substitution show irregular patterns with annealing temperature. In general, changes of the coercive field magnitude are associated with nanoparticle size *i.e.* elimination of domain walls become a single-domain particles and pinning of domain wall [17]. The thermal energy from annealing is used by the nanoparticles to refine the crystallite size. Other thermal energy is also used to redistribute cations that define the final magnetic characteristics. In this experiment, the largest coercive field of H_C = 1,192.2 Oe is obtained for aluminium-substituted cobalt ferrite ($CoAl_xFe_{2-x}O_4$) with x = 0.1 following annealing at 800 °C for 5 hours. The large of the coercive field may contribute to the pinning of the magnetic domain at the interface [7, 17].

4. Conclusions

The structural and magnetic properties of aluminium-substituted cobalt-ferrite nanoparticles synthesised by the co-precipitation method. All the observed XRD peaks could be indexed to cobalt ferrite spinel structure which reveals the absence of impurities. The crystallite size can be varied with the increasing in annealing temperature. The increase of the saturated magnetisation with the annealing temperature is observed. The saturation magnetization reveals the the redistribution of trivalent Fe^{3+} cations in Al substituted cobalt ferrite compare to that of parent cobalt ferrite sample.

Acknowledgments

This study was financially supported by the DIPA Universitas Sebelas Maret in the Republic of Indonesia (Penelitian Mandatory Contract No. 1075/UN27.21/PP/2017).

References

[1] R. K. Kotnala and J. Shah, Handbook of Magnetic Materials (2015) pp 291-379.
[2] I. C. Nlebedim, N. Ranvah, Y. Melikhov, P. I. Williams, J. E. Snyder, A. J. Moses, and D. C. Jiles, J. Appl. Phys. **107**, 09A936 (2010).
[3] L. Kumar and M. Kar, J. Magn. Magn. Mater. **323**, 2042 (2011).
[4] R. Pandit, K. K. Sharma, P. Kaur, R. K. Kotnala, J. Shah, and Kumar, R., J. Phys. Chem. Solids **75**, 558 (2014).
[5] P. N. Anantharamaiah and P. A. Joy, J. Mater. Sci. **50**, 6510 (2015).
[6] B. K. Kuanr, S. R. Mishra, L. Wang, D. DelConte, D. Neupane, V. Veerakumar, and Z. Celinski, Mat. Res. Bull. **76**, 22 (2016).
[7] J. C. Maurya, P. S. Janrao, A. A. Datar, N. S. Kanhe, S. V. Bhoraskar, and V. L. Mathe, J. Magn. Magn. Mater. **412**, 164 (2016).
[8] H. M. Zaki, S. H. Al-Heniti, and A. Hashhash, J. Magn. Magn. Mater. **401**, 1027 (2016).
[9] S. Ansari, H. Arabi, and S. M. Alavi Sadr, J. Supercond. Nov. Magn. **29**, 1525 (2016).
[10] L. Kumar, P. Kumar, M. K. Zope, and M. Kar, J. Supercond. Nov. Magn. **30**, 1629 (2017).
[11] B. G. Toksha, S. E. Shirsath, M. L. Mane, and K. M. Jadhav, Ceram. Int. **43**, 14347 (2017).
[12] P. N. Anantharamaiah and P. A. Joy, J. Phys. D. Appl. Phys. 435005 (2017).
[13] Y. K. Penke, G. Anantharaman, J. Ramkumar, and K. K. Kar, ACS Appl. Mater. Interfaces **9**, 11587 (2017).
[14] B. Purnama, R. Rahmawati, A. T. Wijayanta, and S. Suharyana, J. Magn. **20**, 207 (2015).
[15] S. Amiri and H. Shokrollahi, J. Magn. Magn. Mater. **345**, 18 (2013).
[16] I. C. Nlebedim and D. C. Jiles, J. Appl. Phys. **117**, 17A506 (2015).
[17] D. Jiles, Introduction to Magnetism and Magnetic Materials (1991). doi:10.1007/978-1-4615-3868-4